Electronic structure and optical properties of rhombohedral $CsGeI_3$ crystal

2000 J. Phys.: Condens. Matter 12 9129

(http://iopscience.iop.org/0953-8984/12/43/303)

J. Phys.: Condens. Matter **12** (2000) 9129–9143. Printed in the UK PII: S0953-8984(00)13404-6

Electronic structure and optical properties of rhombohedral $CsGeI_3$ crystal

Li-Chuan Tang, Chen-Shiung Chang† and Jung Y Huang

Institute of Electro-optical Engineering, National Chiao-Tung University Hsinchu, Taiwan, Republic of China

E-mail: u8524806@cc.nctu.edu.tw (Chen-Shiung Chang)

Received 19 April 2000, in final form 31 July 2000

Abstract. We analyse the electronic structure of the perovskite crystal $CsGeI_3$ by means of first-principles calculations and compare our findings to experimental results. Our calculation indicates that $CsGeI_3$ has a direct-transition gap of 0.74 eV at $\vec{k} = (\pi/a)(111)$. The top of the valence bands was found to mainly comprise the 5p orbitals of iodine, while the bottom of the conduction bands is dominated by the 4p orbital of germanium. Photoluminescence (PL) measurements on a single crystal of $CsGeI_3$ indicate two peaks, one at 0.82 μm (1.51 eV) and the other at 1.15 μm (1.08 eV). The shorter-wavelength PL peak is assigned as arising from an interband transition at $\vec{k} = (\pi/a)(111)$ and the longer-wavelength PL is presumably ascribable as originating from a transition involving an energy level within the fundamental band gap. Fourier-transformed infrared spectroscopy reveals that the transparent range of $CsGeI_3$ could extend from $\sim$2 μm to $>$12 μm. The short-wavelength cut-off is mainly limited by the energy band gap, while the long-wavelength limit possibly originates from lattice phonon absorption. Raman spectra of the crystal exhibit two major peaks at 105 cm^{-1} and 151 cm^{-1} and the corresponding overtones at 220 cm^{-1} and 293 cm^{-1}.

1. Introduction

Frequency conversion is a crucial technique for extending laser frequency ranges. To develop this method into an efficient frequency-shifting device, non-linear optical crystals are indispensable. Several useful crystals, including KH_2PO_4 (KDP), $LiNbO_3$, $KTiOPO_4$ (KTP), β-BaB_2O_4 (BBO) and LiB_3O_5 (LBO) [1], have been discovered and successfully utilized for converting laser frequencies to visible and ultraviolet radiation. The situation is quite different in the mid-infrared region, where the non-linear crystals that are efficient at visible wavelengths are not transparent. Lack of material transparency in the mid-infrared is not the only obstacle. Other factors such as the absence of a centre of symmetry and a higher optical damage threshold [2] are also problematic. Therefore, alternative materials have been developed, which include compound semiconductors such as GaSe [3], $AgGaS_2$ [4], $AgGaSe_2$ [5], $ZnGeP_2$ [1, 6], Tl_3AsS_3 [7] and Tl_3AsSe_3 [8]. Although these crystals seem to display suitable non-linearity, they are either difficult to produce or exhibit low optical damage thresholds [9–11].

† Author to whom any correspondence should be addressed. Correspondence address: Institute of Electro-optical Engineering, National Chiao-Tung University, 1001 Ta-Hsueh Road, Hsin-Chu, Taiwan, Republic of China. Telephone: 886-3-5712171, extension 56332; fax: 886-3-5716631.

0953-8984/00/439129+15$30.00

Crystals with a pyramidal basis are known to exhibit a fairly large optical non-linearity. A pyramidal basis in a unit cell contains one tetrahedron with one cation and three anions located at the vertices—such as the pyramidal basis $-As(S/Se)_3$ [12] in $(Tl/Ag)_3As(S/Se)_3$ crystals and $-GeCl_3$ [13, 14] in $CsGeCl_3$ (CGC) crystals. In addition, ternary halides are found to be the potential materials for use in non-linear optical applications [15] and are expected to be transparent in the mid-infrared region (with the exception of the fluorides) [16]. $CsGeI_3$ (CGI), a ternary halide with the space group (SGR) symmetry of $R3m$, possesses a $-GeI_3$ pyramidal basis (figure 1(a)) and therefore is an attractive non-linear crystal for which to seek applications in the infrared region. Its transparency is expected to be wider than that of CGC (0.38–20 μm) [14].

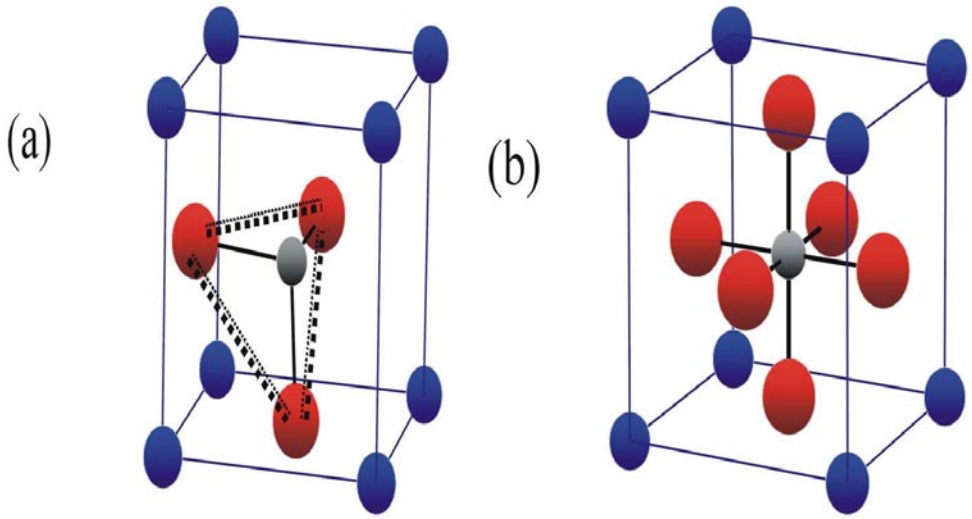

Figure 1. (a) The unit-cell structure of $CsGeI_3$ ($R3m$). In $R3m$ symmetry, the Ge^{2+} ion inclines to one of the corners and a tetrahedron with a Ge^{2+} ion and three I^- ions at vertices to form a pyramidal structure. (b) The unit-cell structure of $CsGeI_3$ ($Pmmm$). In $Pmmm$ symmetry, a Ge^{2+} ion is located at the centre of an octahedron formed by six I^- ions. Medium spheres: Cs; small spheres: Ge; large spheres: I.

(This figure is in colour only in the electronic version, see `www.iop.org`)

The optical damage threshold and the transparent range of materials are related to the magnitude of the band gap, while the optical non-linearity is inversely proportional to the cubic power of the band gap [17]. Clearly, to assess the potential for frequency conversion, it is necessary to understand the electronic band structure of CGI.

The CGI crystal exhibits two different phases at different temperatures. The higher-temperature phase is found to have the symmetry of $Pmmm$, while the lower-temperature phase is found to have $R3m$ symmetry. The phase transition temperature is 290 °C [18]. In this paper, we therefore theoretically analyse the structural stability, electronic and optical properties of CGI with SGR $= R3m$ by means of first-principles calculations and compare them to those of CGI with SGR $= Pmmm$ [18], $CsGeBr_3$ (CGBr, SGR $= R3m$) and CGC (SGR $= R3m$). We also compare the calculated results with experimental results for CGI (SGR $= R3m$), CGC (SGR $= R3m$) [19, 20, 14] and CGBr (SGR $= R3m$) [19, 20, 16].

First-principles calculation based on the Kohn–Sham (KS) density functional theory (DFT) [21] at the local density approximation (LDA) level was employed for calculating the electronic structures of the crystals, using CASTEP (a package developed by Payne's group [22] at

Cambridge University, UK). This Cambridge sequential total-energy package (CASTEP) can perform plane-wave pseudopotential calculations for electronic states of a system with arbitrary atomic arrangement. The calculation yields the ground-state energy and charge density, and enables us to compute any physical quantity related to the total energy.

To improve the transferability of pseudopotentials for different crystal structures, we use a nine-valence-electron non-local pseudopotential for Cs, and employ four- and seven-valence-electron pseudopotentials for Ge and I, respectively. Therefore there are in total 17 occupied bands in our band-structure calculation for CGI with $R3m$ symmetry.

The unit cells of the perovskite crystal CGI with $R3m$ (see figure 1(a)) and $Pmmm$ (figure 1(b)) structures were evaluated; this yielded the lattice parameters $a = b = c = 5.983$ Å, $\alpha = \beta = \gamma = 88.61^\circ$ for $R3m$ symmetry and $a = b = c = 5.83$ Å, $\alpha = \beta = \gamma = 90^\circ$ for $Pmmm$ symmetry. These results are consistent not only with previous reports [18, 19] but also with the x-ray powder diffraction (XRD) data obtained for our CGI crystals. Figure 1(a) shows a unit cell of the crystal structure in the rhombohedral setting. Caesium and iodine ions form a slightly distorted cubic closest packing; germanium is enclosed by a nearly regular iodine octahedron. The Ge atoms are shifted from the centre towards one face of the coordination polyhedron, resulting in the formation of a trigonal antiprism with three short and three long distances [19]. This distortion forms a pyramidal cluster of $–GeI_3$ and results in off-centre symmetry, which results in a high optical non-linear response.

2. First-principles calculations

2.1. Electronic structures

Figure 2(a) shows the calculated electronic band structure of CGI with SGR $= R3m$ and figure 2(b) that for $Pmmm$ structure. Since CGI with SGR $= R3m$ possesses a structure slightly distorted from that of its high-temperature phase, we present our calculated electronic band structure of CGI (SGR $= R3m$) for the same k-points as its high-temperature phase. Like for several ternary halides, e.g. CGC [19, 20, 14], CGBr [19, 20, 16] and $CsSnBr_3$ [23, 24], there is a direct transition at the k-point R for both the cubic primitive phase (high temperature) and the rhombohedral phase. They are found to have energies of 0.74 eV in the low-temperature phase and 0.39 eV in the high-temperature phase. For comparison, we also calculated the corresponding band transition energy at the R point and obtained values of 2.12 eV for $R3m$ CGC and 1.15 eV for CGBr crystals respectively. Schwarz *et al* reported the calculated fundamental gaps at the R point, which were obtained at the Hartree–Fock level, to be 6.71 eV for CGC ($R3m$) and 5.71 eV for CGBr ($R3m$) [20]. Our calculation results are closer to the reported experimental values of 3.67 eV for CGC and 2.32 eV for CGBr [20, 16]. It is well known that the density functional theory scheme underestimates the band gap, while the Hartree–Fock scheme overestimates this value; hence the real band-gap value of CGI is expected to be larger than our calculated value of 0.74 eV.

Fairly isolated flat bands appear around -21 eV and -8 eV. The more dispersive valence bands near the fundamental band gap have a bonding character, which increases in strength with the k-points in the sequence Γ, X, M, R. The lowest of the conduction bands has an antibonding nature with its energy increasing in the sequence Γ, X, M, R. Consequently, the lowest transition energy occurs at the R point. In the Bouckaert–Smoluchowski–Wigner notation [25], the symmetry of the highest occupied band at R can be labelled as R_1. The following unoccupied bands have R_{15} symmetry. We will further investigate the electronic band structure in the next section by resolving the contributions from the atomic orbitals of every atomic species in the unit cell.

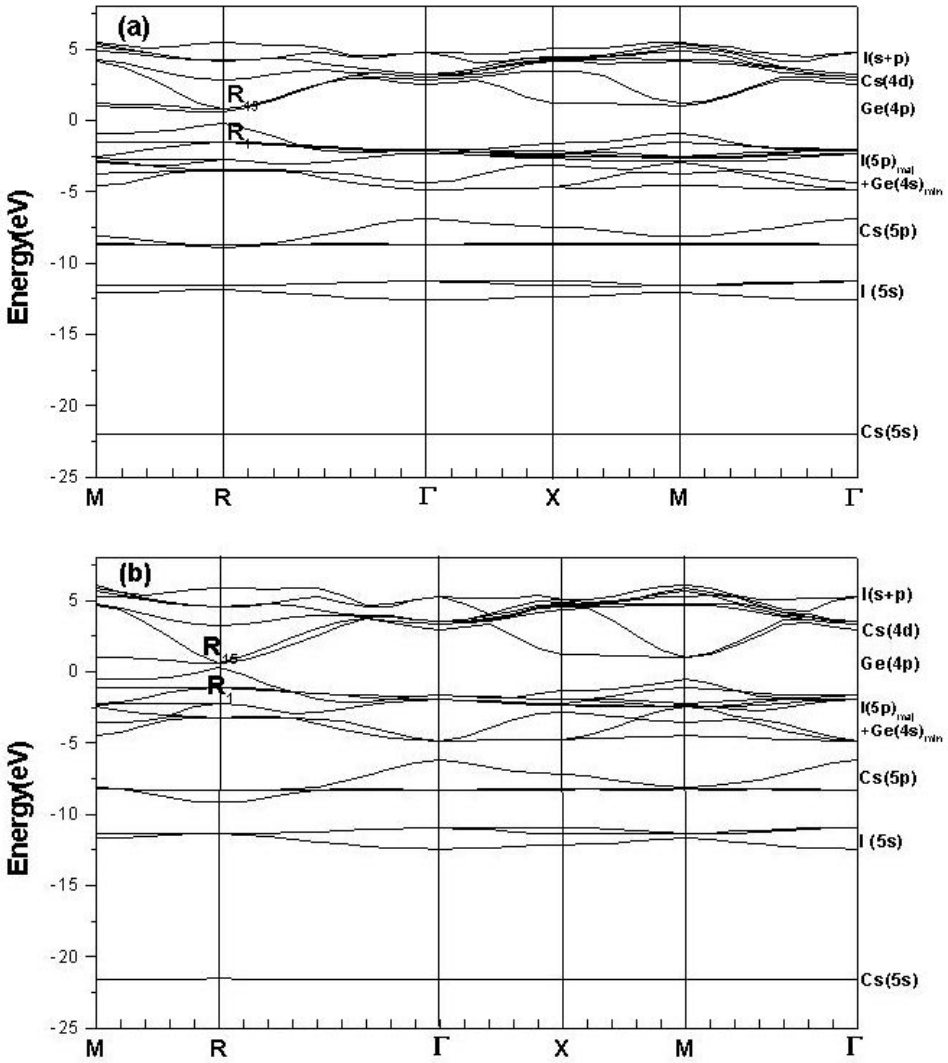

Figure 2. (a) The electronic band structure of $CsGeI_3$ crystal ($R3m$). (b) The electronic band structure of $CsGeI_3$ crystal ($Pmmm$).

2.2. Density of states (DOS)

The investigation of the atomic species and bonding orbitals near the top of the valence bands and bottom of the conduction bands provides valuable information about the nature of the transitions from which the linear and non-linear optical properties of a crystal originate. Calculations of the partial DOS and local DOS can provide such information.

The total density of states (DOS) of a crystal is defined to be the number of states per unit energy interval and per unit volume

$$\mathrm{DOS}(E) = \sum_n \int_{BZ} \mathrm{d}\vec{k}\ \delta[E - E_n(\vec{k})] \tag{1}$$

where $E_n(\vec{k})$ is the nth band energy at $\vec{k}$.

Let $\Psi_{nk}(r)$ be the self-consistent wave function of a crystal at the nth band and k-point in the Brillouin zone (BZ); by following the basic principles of the linear combination of atomic orbitals (LCAO) we can then decompose $\Psi_{nk}(r)$ into a summation over the atomic orbitals (l, m) $\{\Phi_{lm}^{(i)}(r)\}$ of each atomic species (i) in the unit cell:

$$\Psi_{nk}(r) = \sum_{i\in\{\text{atoms}\}} \sum_{l} \sum_{m=-l}^{+l} C_{lm}^{(i)} \Phi_{lm}^{(i)}(r) \tag{2}$$

where

$$C_{lm}^{(i)} = \int_{V_0} \Psi_{nk}(r) \Phi_{lm}^{(i)*} \, \mathrm{d}\vec{r}.$$

The l-orbital of the αth species contributes to $\Psi_{nk}(r)$ [26] a fraction of

$$h_{nk,l}^{(\alpha)} = \left(\sum_{i\in\{\alpha\}} \sum_{m=-l}^{+l} C_{lm}^{(i)} C_{lm}^{(i)*} \right) \Big/ \left(\sum_{i\in\{\alpha,\beta,\gamma,\text{etc}\}} \sum_{l=\{0,1,2,\text{etc}\}} \sum_{m=-l}^{+l} C_{lm}^{(i)} C_{lm}^{(i)*} \right). \tag{3}$$

We can then apply an atom-projection concept for resolving interesting components in the DOS. First, the PDOS from the l-orbital of the αth species can be defined as

$$l_\alpha \, \mathrm{DOS}(E) = \sum_n \int_{BZ} \mathrm{d}\vec{k} \; h_{nk,l}^{(\alpha)} \delta[E - E_n(\vec{k})]. \tag{4}$$

A similar contribution from the l-orbital of the αth species can be further resolved using equation (4) without performing the summation over the orbital angular momentum quantum number l.

Shown in figures 3(a), 4(a) and 5(a) are the calculated PDOS of CGI ($R3m$) from equation (4) for different atomic species, and in figures 3(b), 4(b) and 5(b) we display the results for $Pmmm$ symmetry. In these calculations we set the top of the valence band at 0 eV, and the $R3m$ and $Pmmm$ phases of CGI show similar properties of the PDOS. In short, the 5s and 5p orbitals of Cs contribute only to the lower part of the corelike valence bands, which are located near -21 eV (5s orbital) and -8 eV (5p orbital), respectively, while the 4d orbitals of Cs contribute significantly to the higher conduction bands about 3 eV above their bottom. The atomic species plays a negligible role in the formation of the valence and conduction bands near the fundamental band gap. The top of the valence bands was found to mainly comprise the 5p orbitals of iodine, while the bottom of the conduction bands is dominated by the 4p orbital of germanium.

The energy separation in our calculations at k-points other than R is also obtained. The energies of the $R3m$ phase from the direct transition (i.e. a transition from the bottom of the conduction band to the top of the valence band) are 1.84 eV, 2.83 eV and 4.48 eV at M ($\vec{k} = (\pi/a)(110)$), X ($\vec{k} = (\pi/a)(001)$) and Γ ($\vec{k} = (\pi/a)(000)$), respectively. The corresponding energies of the $Pmmm$ phase are 1.53 eV, 2.47 eV and 5.11 eV.

2.3. The dielectric function ε

The linear optical properties of a material can be obtained from its optical dielectric function, $\varepsilon_{ij}(\vec{q}, \omega)$ at $\vec{q} = 0$. When an incident photon energy is higher than E_g, the photon can be absorbed by the material with an absorption coefficient of $\alpha_{ij}(\omega)$, which can be expressed as the imaginary part of the dielectric function:

$$\begin{aligned} \varepsilon_2^{ij} &= \mathrm{Im}\, \varepsilon_{ij}(\omega) = 4\, \mathrm{Im}\, \chi_{ij}^{(1)} = \frac{\lambda n(\omega)}{2\pi} \alpha_{ij}(\omega) \\ &= \frac{8\pi^2 \hbar^2 e^2}{m^2 V} \sum_k \sum_{cv} (f_c - f_v) \frac{p_{cv}^i(k) \, p_{vc}^j(k)}{E_{vc}^2} \delta[E_{cv}(k) - \hbar\omega] \end{aligned} \tag{5}$$

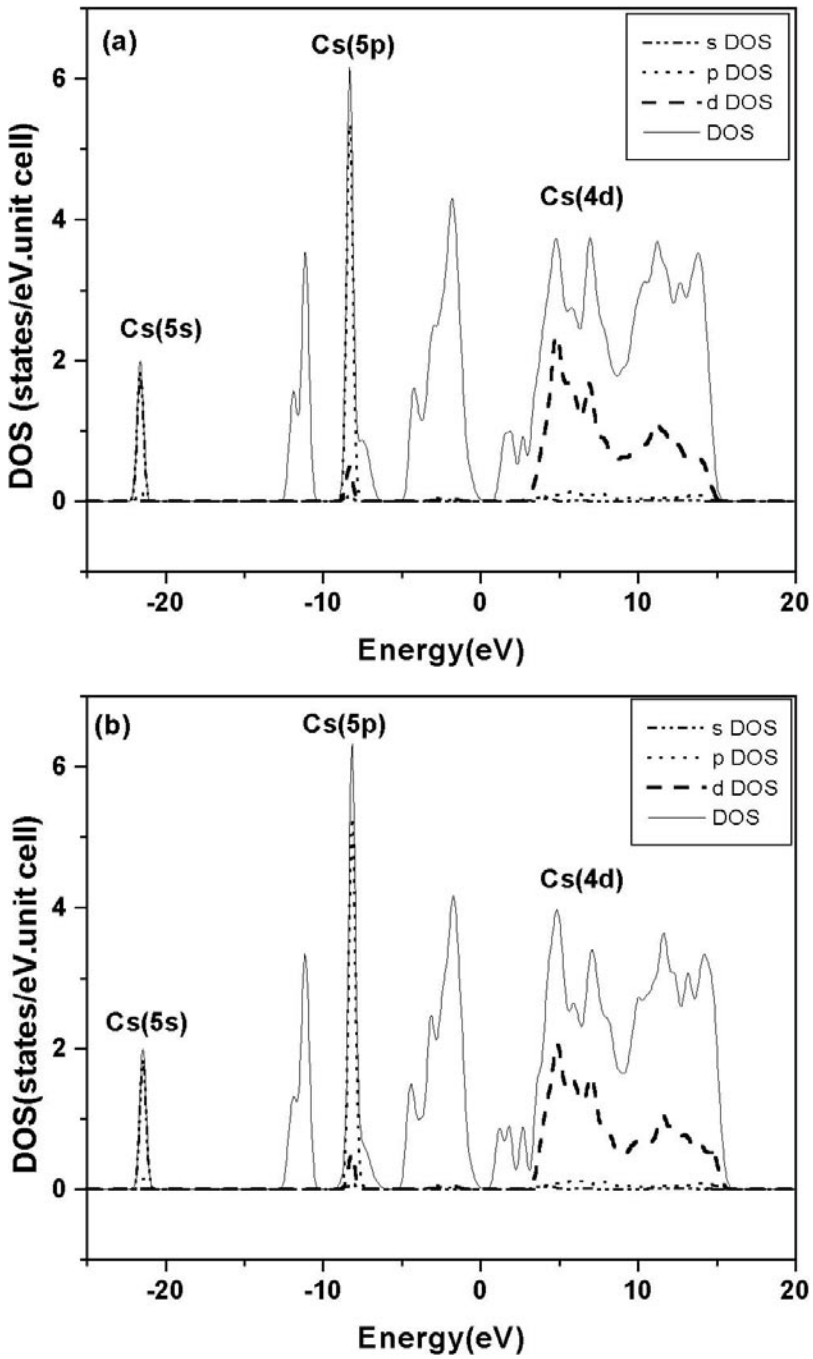

Figure 3. (a) The partial densities of states (DOS) of the Cs-atom contributions in $CsGeI_3$ ($R3m$). (b) The partial densities of states (DOS) of the Cs-atom contributions in $CsGeI_3$ ($Pmmm$).

where $E_{cv}(k) = E_c(k) - E_v(k)$. Here f_c and f_v represent the Fermi distribution functions of the conduction and valence band. The term $p^i_{cv}(k)$ denotes the momentum matrix element

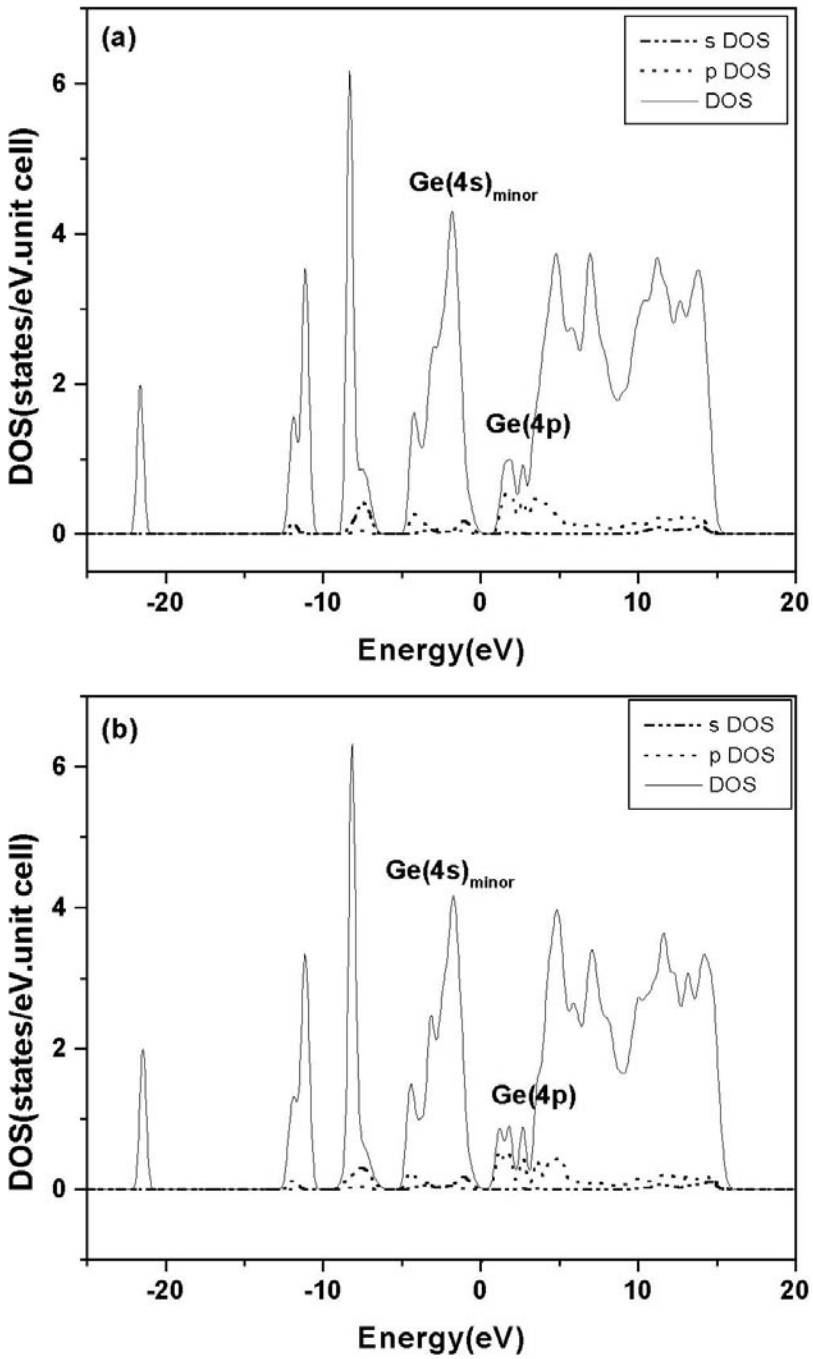

Figure 4. (a) The partial densities of states (DOS) of the Ge-atom contributions in $CsGeI_3$ ($R3m$). (b) The partial densities of states (DOS) of the Ge-atom contributions in $CsGeI_3$ ($Pmmm$).

transition from the energy level c of the conduction band to the level v of the valence band at the kth point in the BZ and V is the volume of the unit cell. The imaginary part of the dielectric

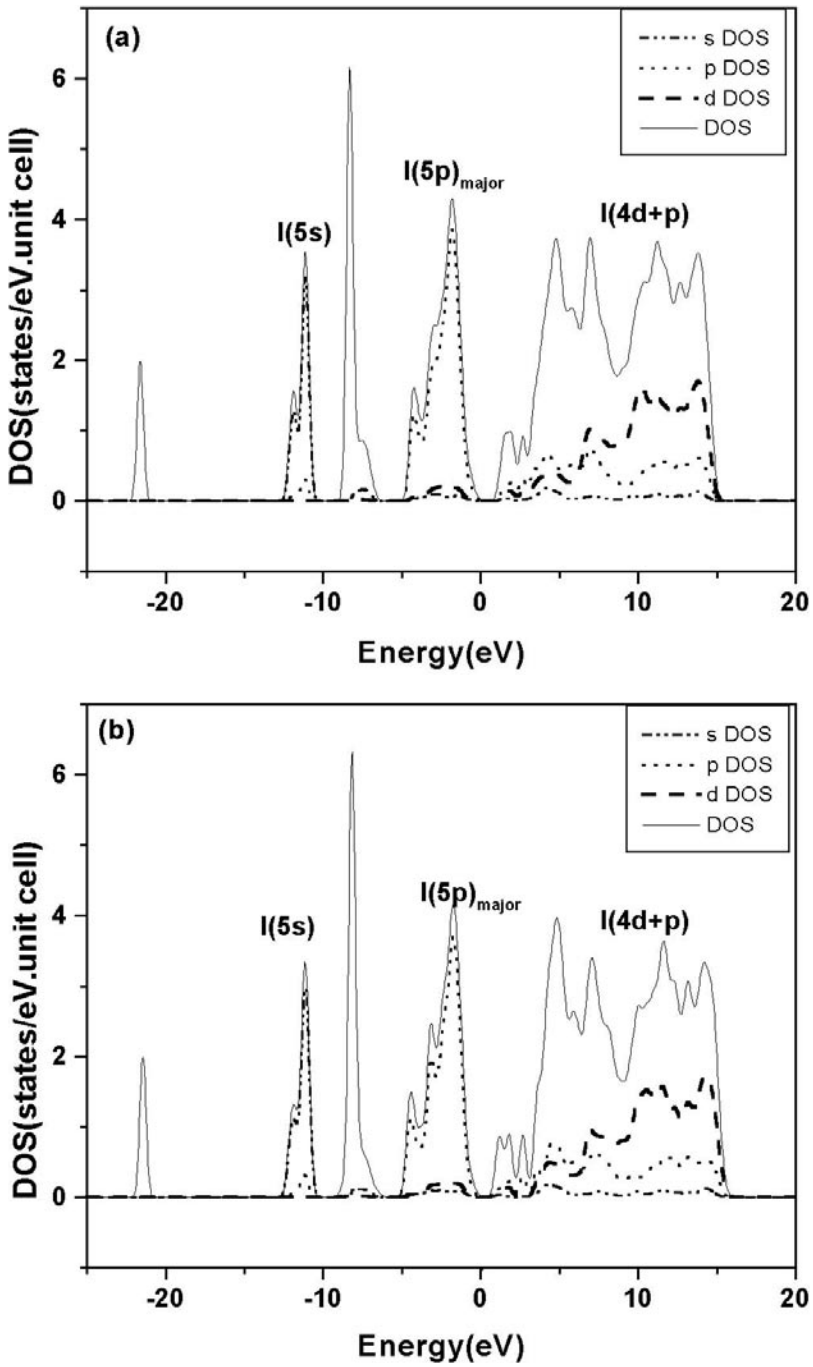

Figure 5. (a) The partial densities of states (DOS) of the I-atom contributions in $CsGeI_3$ ($R3m$). (b) The partial densities of states (DOS) of the I-atom contributions in $CsGeI_3$ ($Pmmm$).

function of CGI ($R3m$ and $Pmmm$) as a function of the incident photon energy was calculated and the results are presented in figures 6(a) and 6(b). The first peak of the imaginary part of

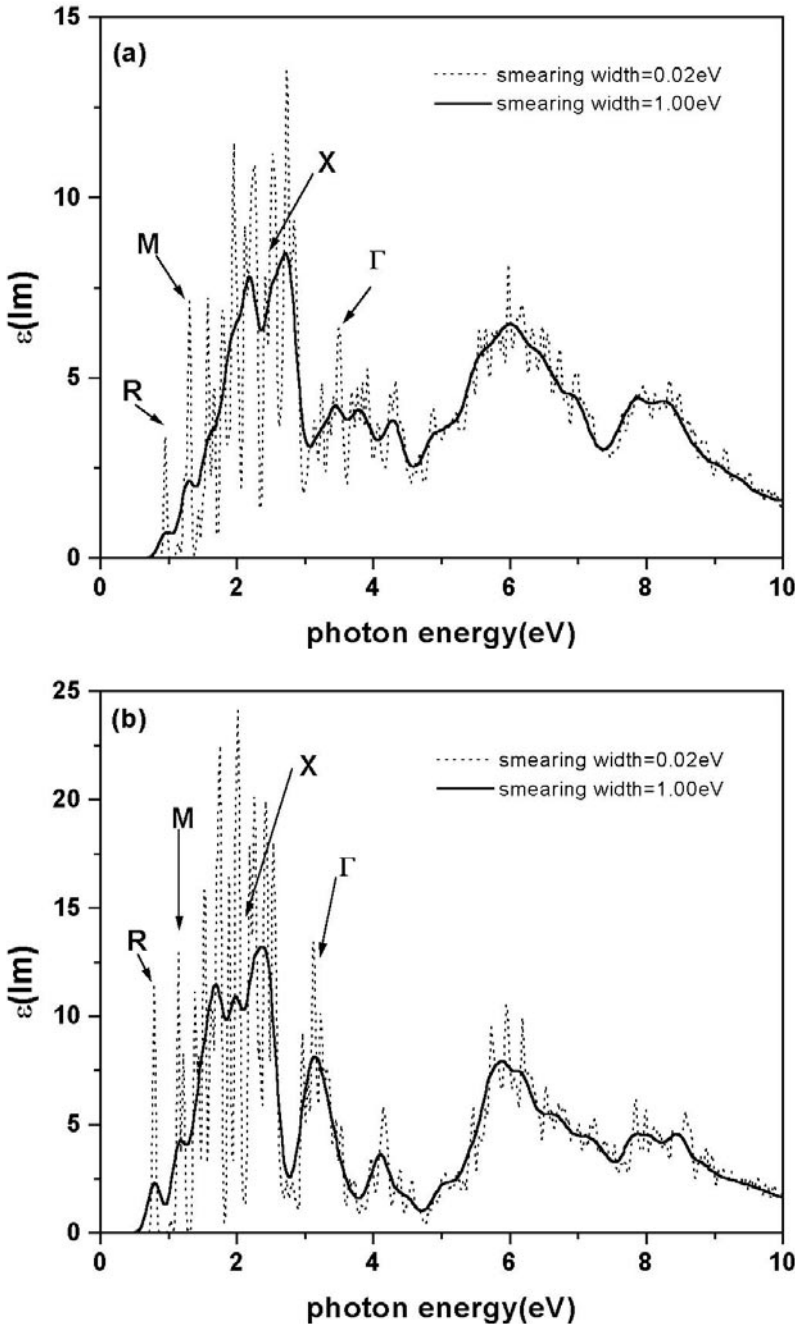

Figure 6. (a) The dispersion of the imaginary part of the dielectric constant in $CsGeI_3$ ($R3m$). (b) The dispersion of the imaginary part of the dielectric constant in $CsGeI_3$ ($Pmmm$).

the dielectric function is due to the transition across the band gap at R. The absorption peaks from the direct transitions at other k-points, such as M, X and Γ, are also labelled in figures 6(a) and 6(b), for comparison.

3. Experiments and results

3.1. Sample preparation and x-ray diffraction pattern

We grew CGI crystals in a three-zone vertical Bridgman furnace. The temperature gradient used was 30 °C cm^{-1} with a pulling rate of 10 mm per day. The CGI crystal was annealed in vacuum at 300 °C for about 100 hours. The colour of the growth product is black. The crystal is very easily decomposed in ambient moisture and at a temperature higher than 150 °C. To characterize the phase of the crystal, we calculated the powder diffraction peaks of CGI ($R3m$) and checked those peaks with the measured XRD powder diffraction pattern. In figure 7, the calculated diffraction pattern of CGI ($R3m$) [27] and the measured x-ray diffraction patterns of the CGI powder and single crystal are presented. Note that the degenerate peaks of [111] and [$1\bar{1}1$] in the $Pmmm$ structure split into two peaks in the $R3m$ phase structure. The same splitting also appears at [220] and [$2\bar{2}0$], but does not emerge in the $Pmmm$ phase (cubic structure). The observed double-peak features near 26° and 43° clearly indicate our crystal sample to have the $R3m$ structure. Note that our result for the $R3m$ phase structure is also consistent with that reported by Thiele *et al* [19] but different from the $Pmmm$ structure data reported by Guen *et al* [18].

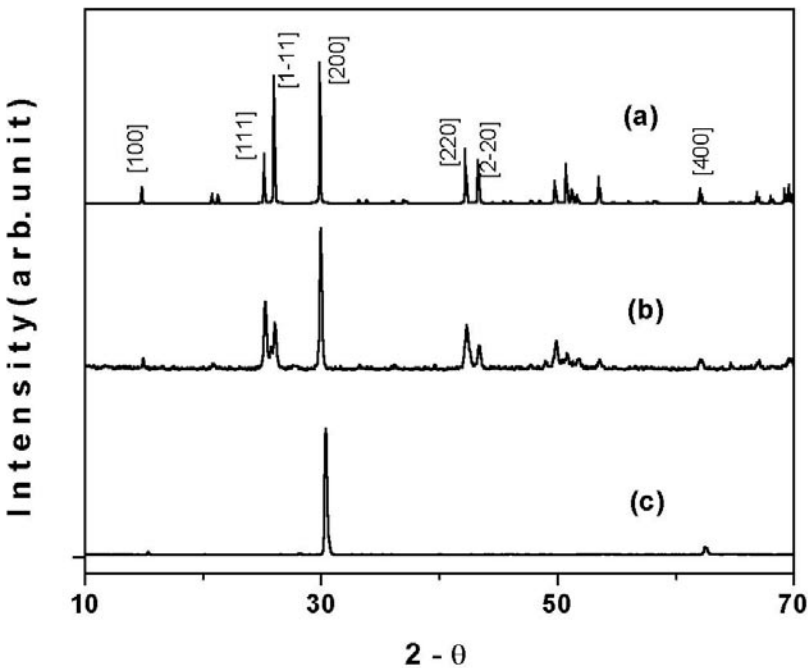

Figure 7. X-ray diffraction patterns (XRD): (a) calculated, (b) for powder and (c) for single-crystal $CsGeI_3$ ($R3m$) obtained using the Cu Kα wavelength.

The single crystal grown for this study is preferentially oriented in the plane [200] (see figure 7(c)); it has a diameter of 1 cm and is 1.5 cm in length. In order to investigate the fundamental band gap in the near-IR and visible ranges, a polished plate was prepared from the ingot for photoluminescence (PL) and absorption measurements. Fourier-transform infrared spectroscopy (FTIR) was further employed to show the transparent range in the mid-IR region. We also use Raman spectroscopy to reveal the crystal lattice properties.

3.2. Optical properties

In the PL measurement, the CGI samples were illuminated with a 15 mW argon-ion laser at a wavelength of 488 nm. The sample was cooled in a vacuum chamber at a temperature of 10 K. The PL spectrum was first taken in a range from 1 μm to 1.8 μm; there is one peak at 1.146 μm (1.08 eV) and a shoulder at 1.118 μm (0.90 eV) (see figure 8(a)). By reference to our calculated electronic band structure, the peak could be attributed as arising from a transition involving an exciton or defect level that lies near the conduction band minimum within the fundamental band gap. We also performed other PL measurements from 0.4 to 1.0 μm (see figure 8(b)). One major PL peak was detected in this region with the peak wavelength varying from 0.82 μm (1.51 eV) at 20 K to 0.714 μm (1.74 eV) at 300 K. As was pointed out in the previous section, DFT theory at the LDA level underestimates a material's band gap. By comparing our calculated transition energy at the R point to experimental results on CGC and CGBr, the calculated values are found to about 40–50% lower than the measured values. Therefore the PL peak at 0.82 μm (1.51 eV, at 20 K) can be confidently attributed as arising from an interband transition at the R point. On the basis of a theoretical study on Si and Ge by Lautenschlager *et al* [28], we see that the observed temperature dependence of the PL energy probably originates from electron–phonon coupling. Of course, thermal expansion of the lattice may also play some role.

We also observed a band-to-band transition at the Γ point from a cathode-ray luminescence measurement (not shown here). A peak position at about 0.32 μm (3.89 eV) was detected.

The result of the FTIR measurement at room temperature is presented in figure 9. There are low transmission onsets when the wavelength of the incident photon is shorter than $\sim$1.2 μm. We estimate the resulting absorption edge to be at 0.73 μm. The absorption is likely to originate from the interband absorption across the fundamental band gap and is consistent with the observed room temperature PL peak at 0.72 μm. The transmission range of the crystal extends to more than 12 μm (limited by our FTIR detection range). The longest infrared transparency wavelength is usually limited by the phonon absorption of the crystal. From the effective-mass concept, the infrared transparency range of CGI is therefore expected to be wider than that of CGC ($\sim$20 μm [14]).

For the Raman scattering measurement, we illuminated the CGI samples with an argon-ion laser at 488 nm with 30 mW average power. The results are presented in figure 10(a). Two Raman peaks with frequencies of 105 cm^{-1} and 151 cm^{-1} were observed. Given that the phonon frequency is inversely proportional to the square root of the mass of GeX_3 (X = Cl, Br, I), our data agree well with the Raman spectra of CGC and CGBr. The results are summarized in table 1. The strongest Raman peaks of the CGI crystal at 105 cm^{-1} and 151 cm^{-1} can therefore be attributed to the symmetric and anti-symmetric stretching modes of the $-GeI_3$ cluster. Another Raman peak occurring at 220 cm^{-1} can be assigned to the corresponding (105 cm^{-1}) overtone. When the sample is excited at 514 nm, the corresponding (151 cm^{-1}) overtone peak at 293 cm^{-1} and the other weak combination tones at 268 cm^{-1} (see figure 10(b)) were more clearly resolved. The low phonon frequencies observed in CGI suggest that its transparency range could be extended into the far-IR region.

4. Conclusions

Detailed theoretical and experimental analyses of CGI crystal are reported. The calculated partial densities of states reveal that the p orbitals from iodine and germanium contribute significantly to the bottom of the conduction bands, while the top of the valence bands is dominated by the p orbital of iodine. A single crystal of CGI had been grown preferentially

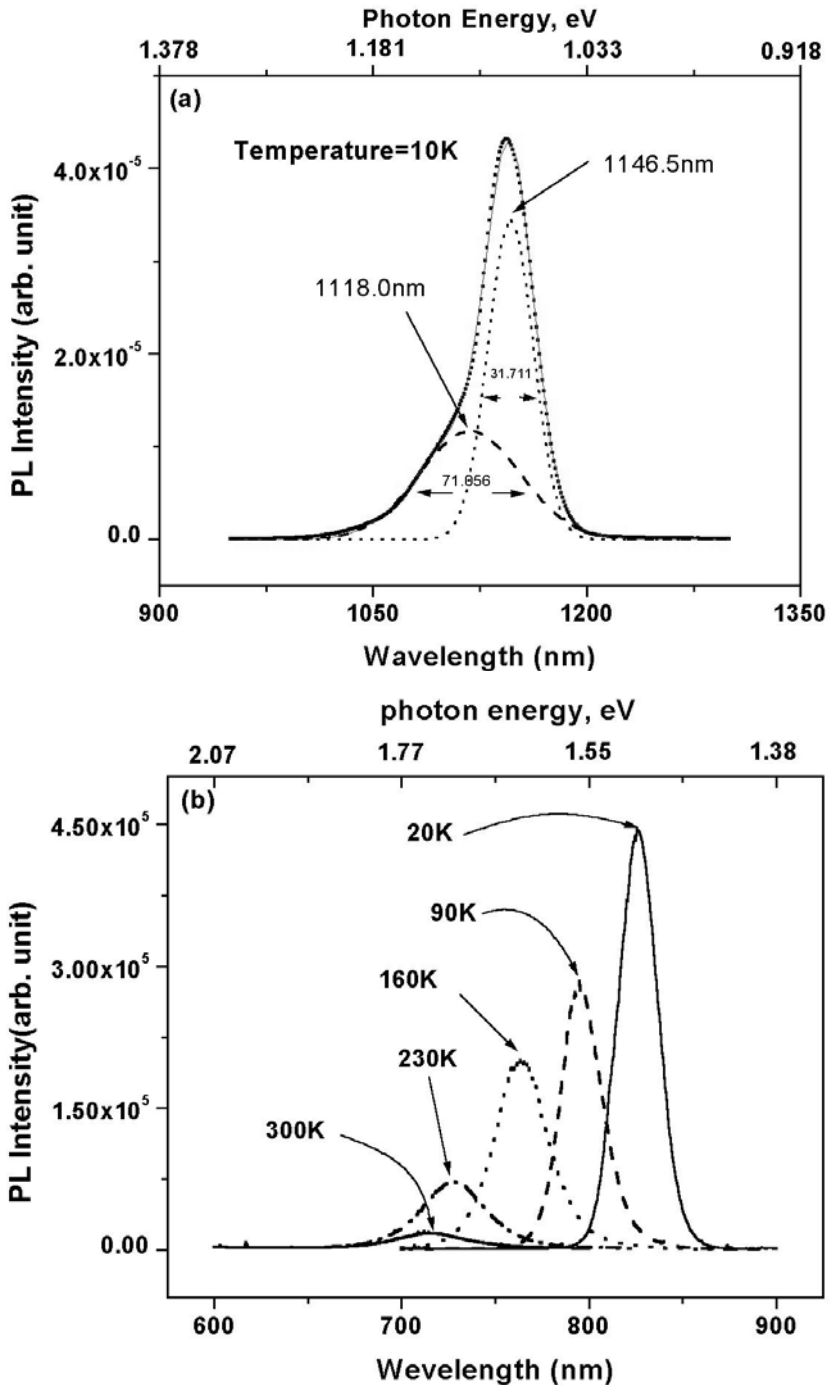

Figure 8. (a) Photoluminescence of $CsGeI_3$ ($R3m$): there are two peaks at 1118 nm and 1146 nm which are detected with a spectral range from 900 nm to 1800 nm at $T = 10$ K. (b) Photoluminescence of $CsGeI_3$ ($R3m$): there are peaks at 820 nm, 793 nm, 770 nm, 729 nm, 714 nm which are detected at $T = 20$ K, 90 K, 160 K, 230 K and 300 K, respectively, with a spectral range from 400 nm to 1000 nm.

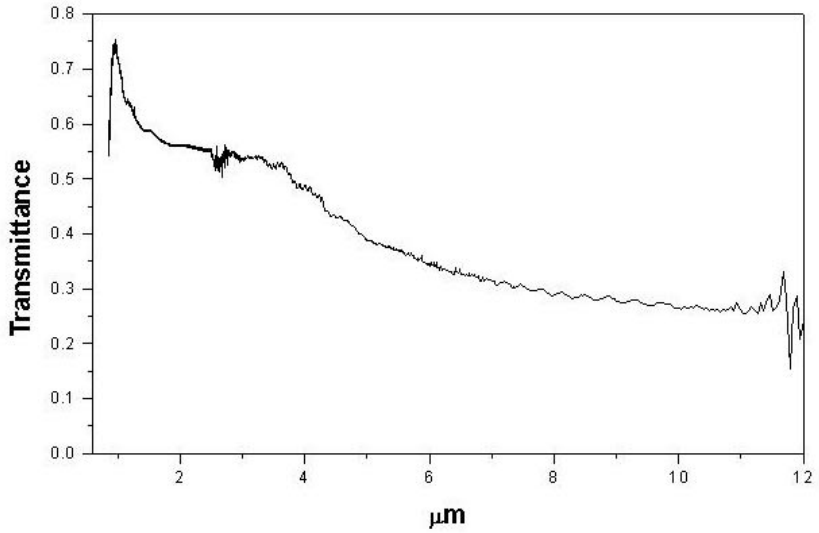

Figure 9. A FTIR spectrum of single-crystal $CsGeI_3$ ($R3m$).

Table 1. The Raman spectra comparison for the ternary halides $CsGeX_3$ (X = Cl, Br and I). The descriptions of the peaks are: 'vs' = very strong; 's' = strong; 'ls' = less strong; 'm' = middle; 'w' = weak; and 'vw' = very weak.

Ternary halides	$CsGeI_3$	$CsGeBr_3$	$CsGeCl_3$	Symmetry	Assignment	Comment
Weight per mole of GeX_3 cluster	453.3	312.3	178.9			
Raman spectra (cm^{-1})	293(m)					Overtone
	268(w)					
	220(m)					Overtone
	151(s)	210(s)	290(s)	A_1	α-GeX_3 stretched	Doubly degenerate
		160(ls)	237(ls)	E		
	105(vs)	139(vs)	200(vs)	A_1	GeX_3 anti-stretched	Doubly degenerate
		91(s)	145(m)			
		77(m)	120(w)			
		49(w)	77(vw)			
			57(m)			

in the [200] plane and its optical properties were investigated with PL, FTIR and Raman spectroscopy. Two photoluminescence peaks—one at 1.15 μm (1.08 eV) and the other at 0.82 μm (1.51 eV)—were detected and could be attributed to transitions involving exciton levels and interband transitions near the R point in k-space. Theoretical calculations of the direct transitions were found to agree with our experimental results. The absorption edge at shorter wavelengths occurs near $\sim$0.73 μm. The transparent limit of the crystal in the infrared region is longer than $\sim$12 μm. Raman shifts at 105 cm^{-1} and 151 cm^{-1} and the corresponding overtone peaks at 220 cm^{-1} and 293 cm^{-1} were detected. Four peaks and a weak feature at 268 cm^{-1} in CGI are attributed as originating from the symmetric and anti-symmetric stretching modes of GeI_3. The assignments are also consistent with the Raman modes in the other ternary halides CGC and CGBr.

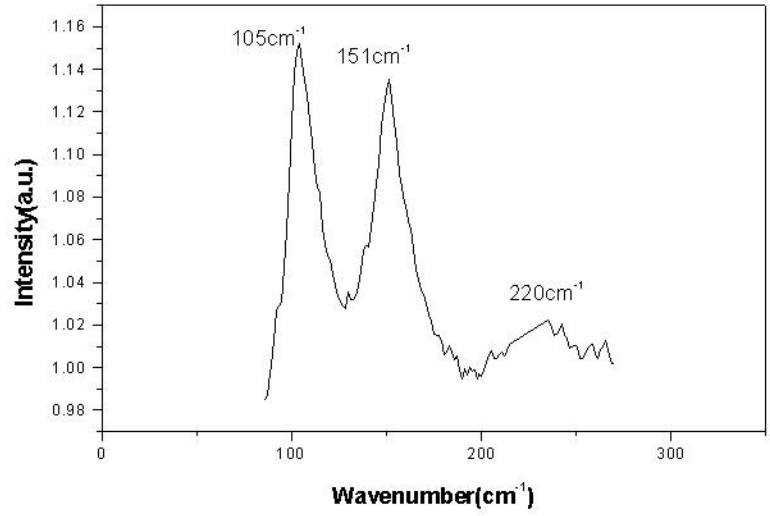

(a)

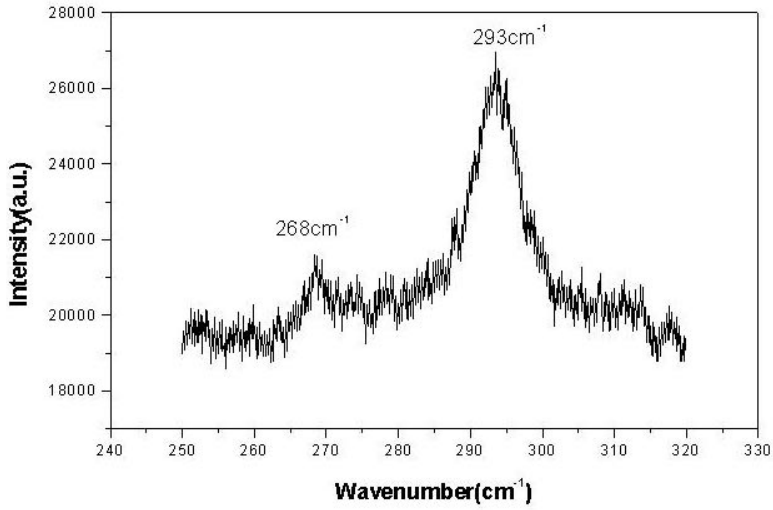

(b)

Figure 10. (a) A Raman spectrum of $CsGeI_3$ ($R3m$) single crystal. $\lambda_{exe} = 488.7$ nm. There are two major peaks, at 105 cm^{-1} and 151 cm^{-1}, detected with a spectral range from 100 cm^{-1} to 200 cm^{-1}. (b) A Raman spectrum of $CsGeI_3$ ($R3m$) single crystal. $\lambda_{exe} = 514.5$ nm. There are two major peaks, at 268 cm^{-1} and 293 cm^{-1}, detected with a spectral range from 250 cm^{-1} to 320 cm^{-1}.

Acknowledgments

This work was supported by the National Science Council (NSC-89-2112-M009-023), ROC. The authors wish to thank Dr Alfa C K Lin and Dr Wen How Lan, Chung-Shan Institute of Science and Technology, for measuring the PL data at various temperatures, and Dr Ming-Hsien Lee, Department of Physics, Tamkang University, for performing the theoretical calculation for the CGI crystal.

References

[1] Dmitriev G, Gurzadyan G G and Nikogosyan D N 1991 *Handbook of Nonlinear Optical Crystals (Springer Topics in Optical Sciences vol 64)* (Berlin: Springer)
[2] Auston D H *et al* 1986 *Appl. Opt.* **26** 211
[3] Cenzual K, Gelato L M, Penzo M and Parthe E 1991 *Acta Crystallogr.* B **47** 433
Boyd L D, Buehler E and Storz F G 1971 *Appl. Phys. Lett.* **18** 301
[4] Kupecek P J, Schwartz C A and Chemla D S 1974 *IEEE J. Quantum Electron.* **10** 540
Bhar G C and Smith R C 1974 *IEEE J. Quantum Electron.* **10** 546
Jaffe J E and Zunger A 1984 *Phys. Rev.* B **29** 1882
Shen Y R 1984 *The Principles of Nonlinear Optics* (New York: Wiley) ch 2
[5] Komine H, Fukumoto J M, Long W H and Stappaerts E A 1994 *CLEO'94 Technical Digest* paper CPD 14-1/31
[6] Mason P D, Jackson D J and Gorton E K 1994 *Opt. Commun.* **110** 163
[7] Feichtner J D and Roland G W 1972 *Appl. Opt.* **11** 993
[8] Suhre D R 1991 *Appl. Phys.* B **52** 367
[9] Buehler E and Wernick J H 1970 *J. Cryst. Growth* **8** 324
[10] Shay J L and Wernick J H 1975 *Ternary Chalcopyrite Semiconductor: Growth, Electronic Properties and Applications* (Oxford: Pergamon) p 244
[11] Yoo K C, Storrick R P, Henningsen T, Spitznagel J A and Hopkins R H 1992 *J. Cryst. Growth* **125** 208
[12] Chemla D S, Kupecek P I and Schwartz C A 1973 *Opt. Commun.* **7** 225
[13] Christensen A N and Rasmussen S E 1965 *Acta Chem. Scand.* **19** 421
[14] Ewbank M D, Cunningham P, Borwick R, Rosker M J and Gunter P 1997 *CLEO'97* paper CFA7, p 462
[15] Hagemann M and Weber H-J 1996 *Appl. Phys.* A **63** 67
[16] Seo D-K, Gupta N, Whangbo M-H, Hillebrecht H and Thiele G 1998 *Inorg. Chem.* **37** 407
[17] Shen Y R 1984 *The Principles of Nonlinear Optics* (New York: Wiley) ch 2
[18] Guen L, Palvadeau P, Spiesser M and Tournoux M 1982 *Rev. Chim. Miner.* **19** 1
[19] Thiele G, Rotter H W and Schmidt K D 1987 *Z. Anorg. Allg. Chem.* **545** 148
[20] Schwarz U, Wagner F, Syassen K and Hillebrecht H 1996 *Phys. Rev.* B **53** 12 545
[21] Jones R O and Gunnarsson O 1989 *Rev. Mod. Phys.* **61** 689
[22] Payne M C, Teter M P, Allan D C, Arieas T A and Joannopoulos J D 1992 *Rev. Mod. Phys.* **64** 1045
[23] Bose S K, Satpathy S and Jepsen O 1993 *Phys. Rev.* B **47** 4276
[24] Lefebvre I, Lippens P E, Lannoo M and Allen G 1990 *Phys. Rev.* B **42** 9174
[25] Bouckaert L P, Smoluchowski R and Wigner E 1936 *Phys. Rev.* **50** 58
[26] Sanchez-Portal D, Artacho E and Soler J M 1996 *J. Phys.: Condens. Matter* **8** 3859
[27] Tang Li-Chuan, Hsu Yu-Kuei, Ko Jui-Feng and Chang Chen-Shiung 2000 *J. Cryst. Growth* to be submitted
[28] Lautenschlager P, Allen P B and Cardona M 1985 *Phys. Rev.* B **31** 2163